NeuroImage 187 (2019) 184–191

Contents lists available at ScienceDirect

NeuroImage

journal homepage: www.elsevier.com/locate/neuroimage

The spatiotemporal pattern of pure tone processing: A single-trial EEG-fMRI study

Qiang Li [a], Guangyuan Liu [a,*], Dongtao Wei [b], Jing Guo [a], Guangjie Yuan [a], Shifu Wu [a]

[a] College of Electronic and Information Engineering, Southwest University, No. 2, TianSheng Street, Beibei, Chongqing 400715, China
[b] Department of Psychology, Southwest University, No. 2, TianSheng Street, Beibei, Chongqing 400715, China

ARTICLE INFO

Keywords:
Single-trial EEG-fMRI
Multi-modal imaging
Pure tone perception
Auditory pathway

ABSTRACT

Although considerable research has been published on pure tone processing, its spatiotemporal pattern is not well understood. Specifically, the link between neural activity in the auditory pathway measured by functional magnetic resonance imaging (fMRI) and electroencephalography (EEG) markers of pure tone processing in the P1, N1, P2, and N4 components is not well established. In this study, we used single-trial EEG-fMRI as a multi-modal fusion approach to integrate concurrently acquired EEG and fMRI data, in order to understand the spatial and temporal aspects of the pure tone processing pathway. Data were recorded from 33 subjects who were presented with stochastically alternating pure tone sequences with two different frequencies: 200 and 6400 Hz. Brain network correlated with trial-to-trial variability of the task-discriminating EEG amplitude was identified. We found that neural responses responding to pure tone perception are spatially along the auditory pathway and temporally divided into three stages: (1) the early stage (P1), wherein activation occurs in the midbrain, which constitutes a part of the low level auditory pathway; (2) the middle stage (N1, P2), wherein correlates were found in areas associated with the posterodorsal auditory pathway, including the primary auditory cortex and the motor cortex; (3) the late stage (N4), wherein correlation was found in the motor cortex. This indicates that trial-by-trial variation in neural activity in the P1, N1, P2, and N4 components reflects the sequential engagement of low- and high-level parts of the auditory pathway for pure tone processing. Our results demonstrate that during simple pure tone listening tasks, regions associated with the auditory pathway transiently correlate with trial-to-trial variability of the EEG amplitude, and they do so on a millisecond timescale with a distinct temporal ordering.

Introduction

Pure tones are typical acoustic stimuli for auditory studies. They are widely used in auditory researches like auditory oddball (Milner et al., 2014), tonotopic mapping (Strainer et al., 1997) and sound pressure researches (Neuner et al., 2014). Although pure tones are the simplest and most basic auditory stimuli, the spatiotemporal pattern of neural activity during the processing of pure tones is incompletely understood. In light of the fundamental role of pure tones in auditory studies, investigating the brain processes underlying pure tone processing is helpful to investigate the processes occurring at different stages of the auditory system and understand the processing mechanisms of brain for complicated acoustic stimuli.

Existing research methods in auditory studies can be divided into invasive methods and noninvasive methods. While invasive methods (Aitkin and Webster, 1971; Rose et al., 1963) could access the dynamic processes of pure tone processing in animal experiments, obtaining comparable data in human subjects is quite challenging. Direct intracranial recordings can only be obtained in neurosurgical patients who require the placement of electrodes as part of their clinical treatment plan (Nourski et al., 2014).

Noninvasive methods such as EEG and fMRI have limitations in their capacity to resolve cortical activity in the time and space dimensions. EEG, with millisecond temporal resolution, is often used to research dynamic neural processes. However, the source localization of EEG is essentially an ill-posed problem. On the contrary, the mm-scale space resolution of fMRI allows localization of both superficial and deep sources of activity, although, its temporal resolution is poor because of the slow nature of the blood-oxygen-level dependent (BOLD) response and the low sampling rate required for the acquisition of the whole-brain fMRI data (Walz et al., 2013).

Combining EEG and fMRI can potentially provide a more sensitive

* Corresponding author.
E-mail address: liugy@swu.edu.cn (G. Liu).

https://doi.org/10.1016/j.neuroimage.2017.11.059
Received 20 June 2017; Received in revised form 23 November 2017; Accepted 26 November 2017
Available online 29 November 2017

measure of neuronal activity based on the complementarity between their temporal and spatial resolutions; the origin of their sources; and the potential capability of fMRI to locate EEG generators, while avoiding the EEG inverse problem (Murta et al., 2015). The fundamental assumption of EEG-fMRI integration approach is that the signals recorded with both modalities are produced by closely interacting, or at least partly overlapping, brain structures (Neuner et al., 2014). It has been suggested that the BOLD signal is governed by local field potentials (LFP) (Murta et al., 2015; Logothetis et al., 2001), which are also regarded to be the basis of neuronal signalling assessed by EEG (Neuner et al., 2014), implying that spatiotemporal data integration can be achieved by investigating correlations between BOLD and scalp EEG. EEG is a selective measure of current source activity which raises energy metabolism, whereas the haemodynamic fMRI signal is related to energy consumption of neural populations. Assuming a linear neurovascular coupling relationship (for healthy young adults) between the hemodynamic response, the LFP and the scalp EEG, the "integration by prediction" approach models the fMRI signal as a function of the EEG convolved with a canonical hemodynamic response function (Mayhew et al., 2010). This approach has proven successful for the treatment of single-trial evoked responses to establish correlations with the BOLD response using the auditory oddball P300 (Eichele et al., 2005) and task relevant ERP components (Walz et al., 2014).

During the past several years, EEG-fMRI integration methods have been used to investigate the neural processes engaged in auditory tasks. However, most of these studies focus on the brain activities related to complex auditory tasks, such as the auditory oddball (Liebenthal et al., 2003; Milner et al., 2014), auditory effortful decision making (Mulert et al., 2008), sound pressure perception (Neuner et al., 2014), task relevant auditory perception (Walz et al., 2015; Puschmann et al., 2016) and auditory attention (Wang et al., 2016). In order to get a more precise spatio-temporal interpretation of the constituent neural processes underlying the simple form of pure tone perception, a passively pure tone listening experiment with neither a complex task nor contrasts between stimulus types (e.g., standards and deviants) needs to be done. (Mayhew et al., 2010) investigated the correlations between the N1/P2 and the BOLD signal and found the activations in the SMA and the STG during P2 in a pure tone listening task. However, it has to be considered that pure tone processing is a complicated process and taking the early and late components into consideration might yield a more comprehensive view of the brain processes underlying it.

In this paper, we used simultaneously recorded EEG and fMRI during a simple listening task to spatially and temporally investigate the pure tone processing pathway. We used the single-trial analysis methodology of Eichele et al. (2005), whereby single-trial event-related potential (ERP) amplitude variability is used to construct the BOLD fMRI univariate model. Instead of focusing on the N1/P2 (Mayhew et al., 2010), we investigated the spatiotemporal evolution for BOLD correlates of auditory ERP components spanning the entire trial. We found a pure tone processing pathway, wherein the midbrain, the primary auditory cortex, and the motor cortex were sequentially activated. Our findings reveal that for the simple pure tone listening task, the auditory pathway is transiently engaged with a distinct temporal ordering and a millisecond timescale.

Material and methods

Participants

FMRI data were collected from 33 right-handed subjects (16 male, 17 female; ages 19–36 years). All subjects had normal hearing thresholds, which were determined by a hearing test administered before scanning by a trained audiologist. Hearing thresholds were better than 20 dB HL in the range between 200 and 6400 Hz. Subjects gave informed consent under a protocol approved by the Institutional Review Board of the Southwest University and were compensated for their participation.

Stimulus presentation

Stimuli were created in Matlab (MathWorks) and were all 0.4 s in duration, with a 44.1 kHz sampling rate and 32 kbit/s rate, and presented during the delay between the acquisition of echoplanar images (EPIs) in a sparse-sampling paradigm. All tones had 10-ms exponential rise and fall envelopes to eliminate acoustic transients. The intensity of all tones was normalized to A-weighted 78 dB. Intensity was measured using a Bruel & Kjaer 2236 sound meter, directly from the same electrostatic earphones used in the MRI scanner placed in an artificial head model. Stimuli were presented in a random order and stimulus-absent "silent" trials were interspersed amongst auditory stimuli within this random order; each kind of stimulus was repeated 72 times. During the experiment subjects were instructed to lie still and listen to the tones. No specific task was performed during the experiment (see Fig. 1).

FMRI acquisition and analyses

Whole brain fMR images were acquired using a 3.0-Tesla Siemens TIM Trio scanner. Functional EPIs were acquired using a sparse-sampling event-related fMRI paradigm: repetition time (TR), 3.4 s; TR delay, 1.4 s; echo time (TE), 26 ms; flip angle, 90°; 32 axial slices; $3 \times 3 \times 3$ mm^3 resolution. A high resolution anatomical scan (MPRAGE) was also performed for each subject with the following parameters: TR, 1900 ms; TE, 2.52 ms; inversion time, 900 ms; flip angle, 9°; 176 sagittal slices; matrix size, 256×256 mm^2; $1 \times 1 \times 1$ mm^3 resolution.

Functional volumes were preprocessed using FreeSurfer (Dale et al., 1999) and custom MATLAB scripts. Volumes were motion-corrected, slice-time-corrected, skull-stripped, linearly detrended, and aligned to anatomical volumes (using FLIRT and bbregister) (Norman-Haignere et al., 2015). Volume data were then resampled to the reconstructed cortical surface computed by FreeSurfer, and smoothed using a 5 mm FWHM kernel to improve signal to noise ratio.

FMRI data for each subject were analyzed in the surface space using FreeSurfer. Data were pooled across sessions. A general linear model (GLM) was applied to each voxel time series. Each of the two conditions was represented by a separate regressor. The model baseline was defined as the no-sound condition. For every regressor, events were modeled as a boxcar representing its duration (0.4 s), convolved with canonical hemodynamic response function, and entered into a multiple regression analysis to generate parameter estimates for each regressor at every voxel.

Group alignment and analyses were conducted in FreeSurfer's averaged_flatten surface space. The results of the single subject analyses, including the estimated coefficients for each condition, were transformed onto the atlas surface and spatially smoothed using a 5-mm Gaussian window calculated across the cortical surface. A random effects group analysis examined differences in the estimated coefficients across subjects using one-way ANOVA. To correct for multiple comparisons, cluster-based thresholding was used (Nichols and Holmes, 2002) with contiguous clusters calculated based on the connectivity of the surface mesh. The data were initially held at a threshold at $p < 0.05$ and then corrected at an alpha level of 0.05.

EEG acquisition and analyses

For the setup of EEG recording, we followed the protocol by Lei et al. (2014). The EEG was measured with a non-magnetic MRI-compatible EEG system (BrainAmp MR plus, Brain products, Munich, Germany). Data was digitized at 5 kHz, and referenced online to FCz. Impedances were kept below 20 kΩ. All 32 electrodes were ring-type sintered nonmagnetic silver/silver chloride (Ag/AgCl) electrodes, placed on the scalp according to the international 10/20 system. An additional electrode was dedicated to the electrocardiogram (ECG). The EEG amplifier, along with a rechargeable power pack was placed about 15 cm outside the bore. The amplified and digitized EEG signal was transmitted via

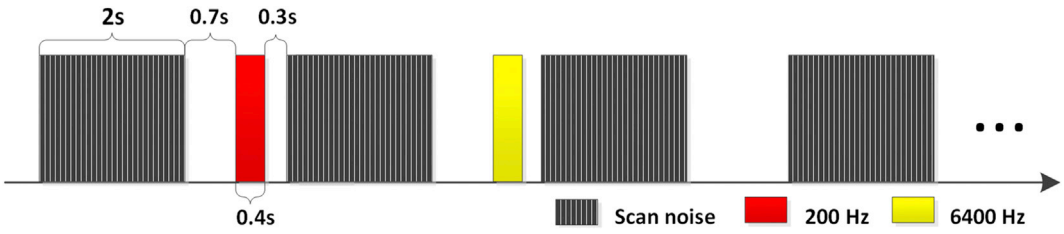

Fig. 1. Stimuli were presented during 144 of the magnetic resonance (MR) volumes, the other 72 vol recorded trials with no auditory stimulation. Tones were either high or low.

fiber optic cables to the recording computer placed outside the scanner room.

EEGs were processed using Analyzer 2.1 software (BrainProducts GmbH, Munich, Germany). MR-gradient and ballistocardiogram (BCG) artifacts were removed using sliding average template subtraction (Allen et al., 2000) and BCG correction was inspected manually. After correction for gradient and BCG artifacts, the data were subsequently down-sampled to 500 Hz and bandpass filtered from 0.1 to 45 Hz with a 50 Hz notch. Independent component analysis (ICA) was performed to eliminate ocular artifacts and residual MR artifacts. After artifact removal, continuous EEG data was re-referenced to averaged TP9/TP10 and segmented into stimulus-locked ERPs. Baseline correction was applied from −200 to 0 ms.

Fusion EEG-fMRI analysis

For EEG-FMRI analysis, we used the single-trial analysis methodology of Eichele et al. (2005) (see Fig. 2). Conjunction analysis between low- and high-frequency was performed to reveal the common spatiotemporal dynamics underlying pure tone processing irrespective of frequency. FMRI data were preprocessed in the mni305 space using SPM12 (Wellcome Trust Centre for NeuroImaging, UCL, London, UK). The preprocessing steps included slice timing, head motion correction, spatial coregistration and normalization, and smoothing. A 10-ms sliding window was used to detect EEG amplitude from −100 to 600 ms (n = 70) around stimulus onset. We calculated the mean amplitude of each trial within this window and took it as its single-trial amplitude. Single-trial amplitude vectors were extracted in a pooled electrode FC1/FC2, where the maximum negativity of N1 was expected. The acquired single-trial amplitude vectors were orthogonalized (Eichele et al., 2005; Mulert et al., 2008) with respect to the vectors of the event onsets and then convolved with the canonical HRF to create the amplitude modulated (AM) regressors. These regressors were introduced into first-level GLM analysis for each subject to compute the fMRI activation maps induced by the single-trial amplitude variability. On the group level, results of the random-effects fMRI analyses are reported using a $p < 0.05$ cluster-extent FWE correction (voxel-height threshold $p < 0.005$).

Results

FMRI results

Statistical maps, showing areas with significant frequency selectivity and color-coded according to the frequency of maximum response, are displayed in Fig. 3. Areas with significant frequency selectivity were found to be confined primarily to the superior temporal plane in both the hemispheres. A prominent low-frequency area with a maximal response to frequencies at 200 (red color) can be observed centrally along the superior temporal plane. It is centered on Heschl's gyrus (HG) and extends along an axis roughly parallel to HG. Two high-frequency areas, responding to frequencies at 6400 Hz (yellow color), are located anterior and posterior to the low-frequency zone. Both of the high-frequency areas extend more medially than the low-frequency area, and completely encircle the low-frequency region medially in left hemisphere. The anterior high-frequency region follows the course of the sulcus anterior to HG. The posterior high-frequency area is located on the superior temporal plane posterior to HG (planum temporale). An additional low-frequency region is present on the lateral posterior STG, or at the lateral edge of the planum temporale, just behind the lateral end of the posterior high-frequency zone.

Average ERPs

Fig. 4A depicts the time courses of the averaged response to each tone, in each condition. After a bilateral frontally distributed P1 (10–30 ms), a

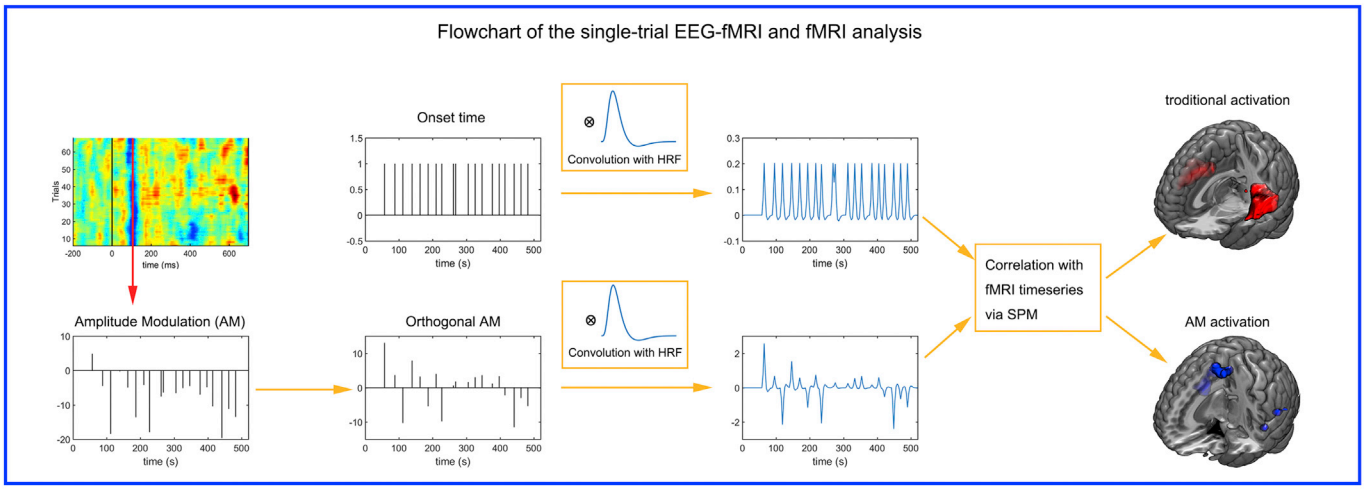

Fig. 2. Flowchart of the single-trial EEG-fMRI and fMRI analysis. AM vectors are derived separately for each time point. To ensure specificity, shared variance between target presentation and AM is removed by orthogonalization. The regressors are convolved with canonical hemodynamic response functions (HRF) to account for the neurovascular coupling before voxelwise correlations with the fMRI signal.

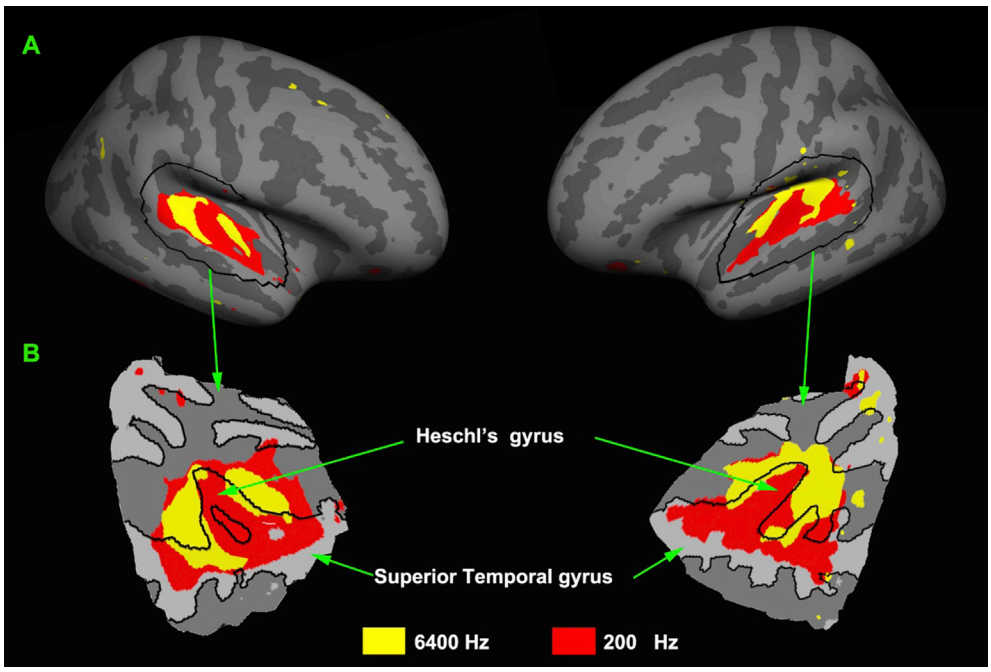

Fig. 3. Group tonotopy maps. (A) Derivation of the flattened patches for average surface, showing the corresponding area on the original surface. (B) Bilateral hemisphere tonotopy map for the group mean projected on a flattened surface. Colored regions are areas that showed significant differences across the two conditions ($p < 0.05$, corrected). Regions are color-coded according to the frequency with the highest amplitude response. On the patch, gyri are represented with lighter shading, and sulci with darker shading.

broad frontocentrally distributed N1 (100–120 ms) emerges, followed by a more central-parietal P2 (200–220 ms) and N4 (430–450 ms). The grand average difference wave of stimulus-locked trials (low-vs. high-frequencies) was inspected at the pooled electrode, FC1/FC2. The stimulus-locked mean amplitudes of low-frequency (200 Hz) in the N1 (100–120 ms) revealed a more pronounced, frontocentrally distributed negativity to high-frequency (6400 Hz) at the electrode, FC1/FC2 ($t(32) = -6.6$, $p < 0.0001$). For 200 Hz, the mean N1 single trial peak latency was detected after 106 ms with a corresponding mean peak amplitude at −6.3 μV. For 6400 Hz, the N1 peak was around 116 ms and the peak amplitude was −2.7 μV. Both low- and high-frequency trials elicited central positive deflections with a mean P2 single trial latency of 210 ms and corresponding mean peak amplitude of 1.1 μV (200 Hz) and 0.2 μV (6400 Hz). The mean amplitude of the low-frequency at FC1/FC2 pointed to more pronounced positivity for low-frequency trials than high-frequency trials ($t(32) = 2.1$, $p = 0.044$). Following this, a negative deflection was found to have emerged in both conditions, peaking at N4 (430–450 ms) with a mean amplitude of −2.2 μV (200 Hz) and −1.9 μV (6400 Hz). In addition, we examined the correlation between P1, N1, P2, and N4 components and there exists correlation between N1 and N4 (Supplementary Table 1 and Table 2).

EEG–fMRI results

Here, we focused on the four prominent components (P1, N1, P2, N4) of ERPs, and three stages: early, middle, and late stages, which were separated according to activation patterns.

The early stage during the P1 (≈30 ms) was located in the midbrain. The parametric modulation by the P1 amplitude revealed a posterior positive activation in the midbrain.

The middle stage during the N1 (≈110 ms) and P2 (≈210 ms) mainly negatively activated the primary auditory cortex and part of the poster-odorsal pathway. In particular, during the N1, the bilateral STG and the supplementary motor area (SMA) were negatively activated; during the P2, the bilateral STG, the bilateral postcentral gyrus (S1) and the supplementary motor area (SMA) were negatively activated. Further positive activations were found in the midbrain for the P2.

The last spatiotemporal stage was related to the N4 (≈440 ms). The parametric modulation by the N4 amplitude revealed a negative midline cluster comprising the SMA and bilateral paracentral lobule. Further positive activations could be found in the midbrain (see Fig. 5 and Table 1).

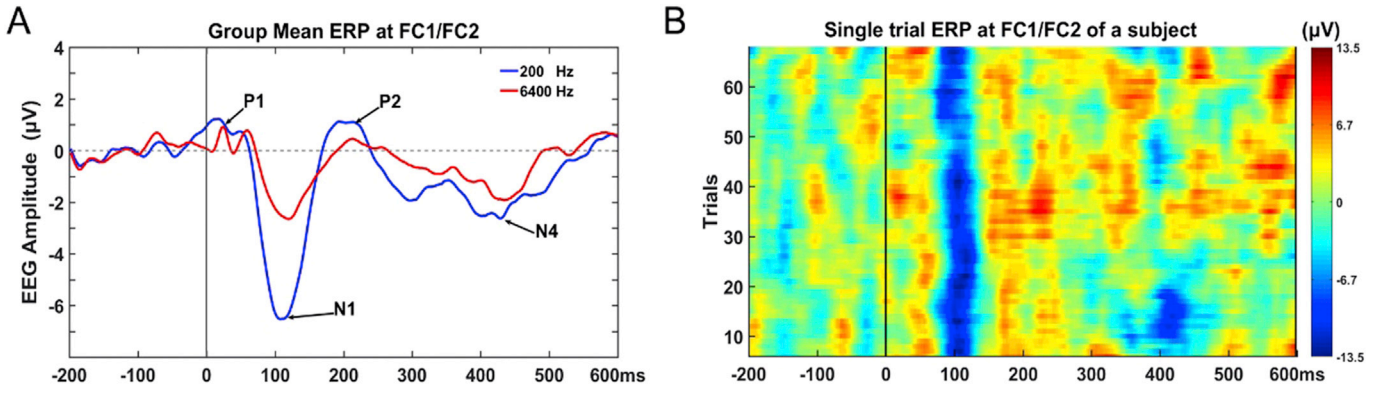

Fig. 4. ERP result. (A) The grand average wave form of high and low frequencies at FC1/FC2. (B) Typical single-trial data at FC1/FC2 during the listening task of 200 Hz.

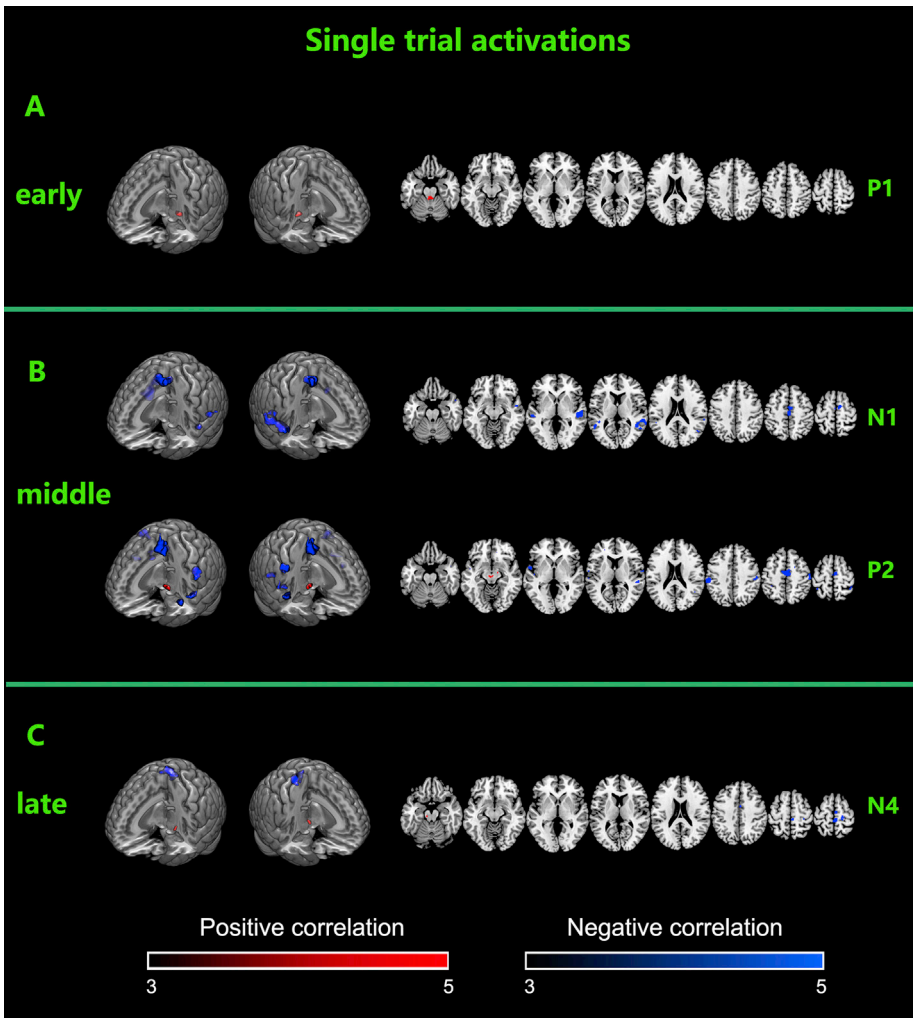

Fig. 5. Single-trial coupling fMRI-EEG analysis for 3 time windows in the listening task. (A) Early window (P1), MB was activated in the task for both frequencies. (B) Middle window (N1-P2), STG, SMA, and S1 were negatively activated. (C) SMA was negatively activated in the late window (N4). All AM-related activations were held at a threshold at $p < 0.05$ cluster-extent FWE correction (voxel-height threshold $p < 0.005$). MB = middle brain; STG = the superior temporal gyrus; SMA = the supplementary motor area; S1 = the primary somatosensory cortex.

Discussion

Here, we used single trial EEG-fMRI in combination with standard ERP and fMRI analyses to investigate the temporal and spatial course of pure tone perception. For each time window, we constructed fMRI regressors based on trial-to-trial fluctuations of the EEG amplitude and used these to model the trial-to-trial variability of events. These regressors were combined with traditional event-related regressors to model transient and mean activations. All such regressors were convolved with a canonical hemodynamic response function and used as explanatory variables in a general linear model analysis of fMRI.

The traditional event related regressors produced a contrast similar to that previously seen for this task (Humphries et al., 2010). Contrastingly, trial-to-trial variability yielded focally distinct hemodynamic activations that could not be explained by traditional event-related modeling. Our primary finding of the single-trial ERP-fMRI was the processing stream of pure tone perception, which consists of three stages.

The midbrain was found to be activated in both frequencies during P1 (≈30 ms), forming the first response stage. The early series of ERPs recorded in the initial 40 msec following the auditory stimulus has been attributed to activations of the brainstem, midbrain, and thalamus auditory nuclei (Picton et al., 1974; Jewett and Williston, 1971). The midbrain is a key part of the auditory pathway (Stockard and Rossiter, 1977; Saenz and Langers, 2014) and is well-known for its function of receiving sensory signals and sending them to primary cortical regions, i.e., the cochlear nuclear complex gives rise to widespread projections to nuclei throughout the midbrain (Cant and Benson, 2003). (Schreiner and Langner, 1997) found tonotopic progressions in the auditory midbrain, indicating that the midbrain plays a more complex function than simply forwarding auditory signals. Our fusion results in this time window support this speculation and suggest that the midbrain plays a key role during the early (P1) time window.

The second spatiotemporal stage during N1 (≈110 ms) and P2 (≈210 ms) was mainly located in the STG, SMA, S1, and the midbrain. Previous EEG–fMRI studies have localised the N1 and P2 with bilateral dipoles or current source density maps in the STG (Mulert et al., 2004; Scarff et al., 2004; Debener et al., 2007, 2008; Mayhew et al., 2010; Milner et al., 2014). Considerable traditional fMRI research (Talavage et al., 2004; Wessinger et al., 1997; Thomas et al., 2015; Leaver and Rauschecker, 2016; Humphries et al., 2010; Ahveninen et al., 2016; Bilecen et al., 1998, 2002) has shown that the STG is the core region that responds to auditory stimuli, indicating the key role of STG in the auditory pathway. Moreover, intracranial EEG recording (Nourski et al., 2014) in the STG has documented the strongest activation in the same peak latency range of N1 and P2. In particular, several researches have suggested that N1 and P2 are generated in the STG (Ponton et al., 2002; Shahin et al., 2003; Pantev et al., 1988; Hari et al., 1982; Näätänen and Picton, 1987; Maess et al., 2007).

Table 1
EEG–fMRI single trial analysis.

Components	Region	Cluster size[a]	T	+/-	MNI coordinates		
					x	y	z
P1	Midbrain	45	7.59	pos	−2	−34	−24
N1	L Superior Temporal Gyrus	18	5.98	neg	−52	−10	−14
	R Superior Temporal Gyrus	34	7.47	neg	48	−8	−8
	R Superior Temporal Gyrus	533	9.12	neg	52	−20	−2
	L Superior Temporal Gyrus	56	8.75	neg	−58	−26	2
	L Superior Temporal Gyrus	25	6.64	neg	−42	−42	8
	L Superior Temporal Gyrus	66	6.83	neg	−52	−52	−8
	R Superior Temporal Gyrus	58	5.97	neg	46	−62	16
	L Superior Temporal Gyrus	46	5.50	neg	−64	−34	12
	R SMA	291	7.88	neg	−2	−16	56
	L SMA	47	5.94	neg	2	28	−72
P2	Midbrain	42	6.80	pos	0	−18	−14
	L Superior Temporal Gyrus	48	6.49	neg	−54	2	0
	L Superior Temporal Gyrus	61	8.08	neg	−62	−16	8
	R Superior Temporal Gyrus	50	8.39	neg	44	−28	6
	R Superior Temporal Gyrus	90	7.40	neg	−66	−8	8
	R Superior Temporal Gyrus	62	5.92	neg	−48	−52	16
	L Postcentral Gyrus	209	7.22	neg	−54	−26	42
	R Postcentral Gyrus	173	8.16	neg	54	−12	50
	L&R SMA	327	8.96	neg	6	−10	58
	R Postcentral Gyrus	14	5.94	neg	40	−46	62
	R Postcentral Gyrus	10	4.91	neg	18	−48	72
N4	Midbrain	13	5.16	pos	−10	−26	−14
	SMA	249	6.45	neg	4	−16	66
	L&R Paracentral Lobule	37	6.25	neg	4	−32	68

[a] Number of voxels exceeding a voxel-height threshold of $p < 0.005$ using a $p < 0.05$ cluster-extend FWE correction.

It is worth noting that motor areas, in particular the SMA and S1, were activated in this stage. The EEG-fMRI study of Mayhew et al. (2010) supports our findings that the SMA and S1 were activated during P2. Although the SMA and S1 have been intensely investigated in relation to their motor functions, they are also consistently reported in studies of auditory processing (Lima et al., 2016). The SMA has been reported to be commonly activated in auditory perceptual and auditory imagery studies, even when the tasks do not involve overt motor components (Warren et al., 2006; Pereira et al., 2011; McGettigan et al., 2015). S1 is also found to be activated in pure tone and speech perception tasks (Tzourio et al., 1997; Cogan et al., 2014). There are structural and functional connections between the SMA, S1, and regions that are considered to be central for sound and speech processing (Catani et al., 2012; Reznik et al., 2015; Vergani et al., 2014; Rauschecker and Tian, 2000). Moreover, the SMA and S1 are involved in the posterodorsal auditory pathway, which is important for aspects of sensorimotor integration and spatial processing ("how/where") (Rauschecker, 2011; Rauschecker and Scott, 2009; Scott and Johnsrude, 2003). The activation of the SMA and S1 in this stage indicates that during the middle time window, along with the primary auditory cortex, the posterodorsal auditory pathway also takes part in the processing of pure tone.

The last spatiotemporal stage is related to N4 (≈440 ms), and yielded activations in the SMA and the midbrain. The midbrain was therefore found to include all three stages' representations in this study. Later components in the ERPs are often attributed to "endogenous'' or "top-down'' processing (Wijers, 1995). Some models of brain function in the context of perceptual inference and learning focus on the hierarchical nature of cortical systems and suggest that these components derive from high levels of processing (Näätänen, 1992; Friston, 2005). We therefore expect that the regionally specific correlates of N4 would most likely be located outside the sensory region in multimodal higher-order cortical areas. The regional deployment of our activations conformed roughly to our general prediction that the N4 is coherent with metabolic or synaptic activity in higher cortical areas. The activation of SMA in this stage suggested the sustained participation of the posterodorsal auditory pathway in the middle and late stages of pure tone processing. Hierarchical organization in the cerebral cortex combines elements of serial processing: lower cortical areas with simpler receptive-field organization, such as the primary auditory cortex, project to higher areas with increasingly complex response properties, such as the motor cortex (Rauschecker and Scott, 2009). This theory could explain the disappearance of the STG in this stage, since it may have projected the auditory stimuli to a complex response region: the SMA.

The sign (pos/neg) of the correlation between the components and BOLD should be noticed. Evoked potentials are a stimulus induced, transient change in the ongoing EEG signal, created by time-locked neural activities over a relatively small time window. They reflect the summation of synchronously active and spatially aligned cortical pyramidal cells (Speckmann and Elger, 2004), and in addition are sensitive to the dendrite orientation, conduction through the brain and skull (Mayhew et al., 2010). The EEG recorded in this study are therefore a complex representation of the total neural activity and the current orientations in different regions could be opposite. In contrast, the BOLD fMRI signal integrates timelocked and non-time-locked neural activities from the entire neuronal population regardless of the orientation, or excitatory or inhibitory designation of those neurons (Logothetis et al., 2001). The different formation mechanism of the EEG and BOLD signals, especially the different current source orientations in different brain regions, could provide a reason for the difference in the sign (pos/neg) of the correlation between the STG, SMA and midbrain in this study.

Conclusions

In conclusion, this is the first simultaneous EEG–fMRI coupling study that has looked at the processing stream of pure tone processing, capitalizing on the high temporal resolution of ERPs and the high spatial resolution of fMRI. We found the pure tone processing stream projected from the midbrain to the primary auditory cortex and then to the motor cortex. The regions identified as sensitive to pure tone stimuli in all three sequential spatiotemporal stages are consistent with the regions identified in the literature for the auditory pathway (Ehret and Romand, 1997; Rees and Palmer, 2010; Saenz and Langers, 2014). Moreover, our results review the active timings of the midbrain, the primary auditory cortex, and the motor cortex during pure tone perception, composing a complete auditory spatiotemporal processing pathway.

Acknowledgements

This research was supported by the National Natural Science Foundation of China (61472330).

Appendix A. Supplementary data

Supplementary data related to this article can be found at https://doi.org/10.1016/j.neuroimage.2017.11.059.

References

Ahveninen, J., et al., 2016. Intracortical depth analyses of frequency-sensitive regions of human auditory cortex using 7T fMRI. NeuroImage 143, 116–127. Available at: http://www.sciencedirect.com/science/article/pii/S1053811916304712.

Aitkin, L.M., Webster, W.R., 1971. Tonotopic organization in the medial geniculate body of the cat. Brain Res. 26 (2), 402–405. Available at: http://www.sciencedirect.com/science/article/pii/S000689937180015X.

Allen, P.J., Josephs, O., Turner, R., 2000. A method for removing imaging artifact from continuous EEG recorded during functional MRI. NeuroImage 12 (2), 230–239. Available at: http://www.sciencedirect.com/science/article/pii/S1053811900905998.

Bilecen, D., et al., 2002. Amplitopicity of the human auditory cortex: an fMRI study. NeuroImage 17 (2), 710–718.

Bilecen, D., et al., 1998. Tonotopic organization of the human auditory cortex as detected by BOLD-FMRI. Hear. Res. 126 (1–2), 19–27. Available at: http://www.ncbi.nlm.nih.gov/pubmed/9872130.

Cant, N.B., Benson, C.G., 2003. Parallel auditory pathways: projection patterns of the different neuronal populations in the dorsal and ventral cochlear nuclei. Brain Res. Bull. 60 (5–6), 457–474. Available at: http://www.sciencedirect.com/science/article/pii/S0361923003000509.

Catani, M., et al., 2012. Short frontal lobe connections of the human brain. Cortex 48 (2), 273–291. Available at: http://www.sciencedirect.com/science/article/pii/S0010945211003170.

Cogan, G.B., et al., 2014. Sensory-motor transformations for speech occur bilaterally. Nature 507 (7490), 94–98. Available at: https://doi.org/10.1038/nature12935.

Dale, A.M., Fischl, B., Sereno, M.I., 1999. Cortical surface-based analysis: I. Segmentation and surface reconstruction. NeuroImage 9 (2), 179–194. Available at: http://www.sciencedirect.com/science/article/pii/S1053811998903950.

Debener, S., et al., 2008. Corrigendum to: “Towards single-trial analysis in cognitive brain research.” Trends Cognitive Sci. 12 (1), 6. Available at: http://www.sciencedirect.com/science/article/pii/S1364661307003075.

Debener, S., et al., 2007. Improved quality of auditory event-related potentials recorded simultaneously with 3-T fMRI: removal of the ballistocardiogram artefact. NeuroImage 34 (2), 587–597. Available at: http://www.sciencedirect.com/science/article/pii/S1053811906009827.

Ehret, G., Romand, R., 1997. The Central Auditory System. Oxford University Press, USA.

Eichele, T., et al., 2005. Assessing the spatiotemporal evolution of neuronal activation with single-trial event-related potentials and functional MRI. Proc. Natl. Acad. Sci. U. S. A. 102 (49), 17798–17803. Available at: http://www.pubmedcentral.nih.gov/articlerender.fcgi?artid=1295592&tool=pmcentrez&rendertype=abstract.

Friston, K., 2005. A theory of cortical responses. Phil. Trans. R. Soc. B Biol. Sci. 360 (1456), 815 LP–836. Available at: http://rstb.royalsocietypublishing.org/content/360/1456/815.abstract.

Hari, R., et al., 1982. Interstimulus interval dependence of the auditory vertex response and its magnetic counterpart: implications for their neural generation. Electroencephalogr. Clin. Neurophysiol. 54 (5), 561–569. Available at: http://www.sciencedirect.com/science/article/pii/0013469482900414.

Humphries, C., Liebenthal, E., Binder, J.R., 2010. Tonotopic organization of human auditory cortex. NeuroImage 50 (3), 1202–1211. Available at: https://doi.org/10.1016/j.neuroimage.2010.01.046.

Jewett, D.O.N.L., Williston, J.S., 1971. Auditory-evoked far fields averaged from the scalp of humans. Brain 94 (4), 681–696. Available at: https://doi.org/10.1093/brain/94.4.681.

Leaver, A.M., Rauschecker, J.P., 2016. Functional topography of human auditory cortex. J. Neurosci. 36 (4), 1416–1428. Available at: http://www.jneurosci.org/cgi/doi/10.1523/JNEUROSCI.0226-15.2016.

Lei, X., et al., 2014. Brain scale-free properties in awake rest and NREM sleep: a simultaneous EEG/fMRI study. Brain Topogr. 28 (2), 292–304.

Liebenthal, E., et al., 2003. Simultaneous ERP and fMRI of the auditory cortex in a passive oddball paradigm. NeuroImage 19 (4), 1395–1404. Available at: http://www.sciencedirect.com/science/article/pii/S1053811903002283.

Lima, C.F., Krishnan, S., Scott, S.K., 2016. Roles of supplementary motor areas in auditory processing and auditory imagery. Trends Neurosci. 39 (8), 527–542. Available at: http://www.sciencedirect.com/science/article/pii/S0166223616300546.

Logothetis, N.K., et al., 2001. Neurophysiological investigation of the basis of the fMRI signal. Nature 412 (6843), 150–157. Available at: https://doi.org/10.1038/35084005.

Maess, B., et al., 2007. Localizing pre-attentive auditory memory-based comparison: magnetic mismatch negativity to pitch change. NeuroImage 37 (2), 561–571. Available at: http://www.sciencedirect.com/science/article/pii/S1053811907004624.

Mayhew, S.D., et al., 2010. EEG signatures of auditory activity correlate with simultaneously recorded fMRI responses in humans. NeuroImage 49 (1), 849–864. Available at: http://www.sciencedirect.com/science/article/pii/S1053811909006302.

McGettigan, C., et al., 2015. Individual differences in laughter perception reveal roles for mentalizing and sensorimotor systems in the evaluation of emotional authenticity. Cereb. Cortex 25 (1), 246–257. Available at: https://doi.org/10.1093/cercor/bht227.

Milner, R., et al., 2014. Towards neural correlates of auditory stimulus processing: a simultaneous auditory evoked potentials and functional magnetic resonance study using an odd-ball paradigm. Med. Sci. Monit. 20, 35–46. Available at: http://www.medscimonit.com/abstract/index/idArt/889712.

Mulert, C., et al., 2004. Integration of fMRI and simultaneous EEG: towards a comprehensive understanding of localization and time-course of brain activity in target detection. NeuroImage 22 (1), 83–94. Available at: http://www.sciencedirect.com/science/article/pii/S1053811904000084.

Mulert, C., et al., 2008. Single-trial coupling of EEG and fMRI reveals the involvement of early anterior cingulate cortex activation in effortful decision making. NeuroImage 42 (1), 158–168. Available at: http://www.sciencedirect.com/science/article/pii/S1053811908005120.

Murta, T., et al., 2015. Electrophysiological correlates of the BOLD signal for EEG-informed fMRI. Hum. Brain Mapp. 36 (1), 391–414.

Näätänen, R., 1992. Attention and Brain Function. Psychology Press.

Näätänen, R., Picton, T., 1987. The N1 wave of the human electric and magnetic response to sound: a review and an analysis of the component structure. Psychophysiology 24 (4), 375–425. Available at: https://doi.org/10.1111/j.1469-8986.1987.tb00311.x.

Neuner, I., et al., 2014. Cortical response variation with different sound pressure levels: a combined event-related potentials and FMRI study. PLoS One 9 (10), e109216. Available at: http://www.pubmedcentral.nih.gov/articlerender.fcgi?artid=4184873&tool=pmcentrez&rendertype=abstract.

Nichols, T.E., Holmes, A.P., 2002. Nonparametric permutation tests for functional neuroimaging: a primer with examples. Hum. Brain Mapp. 15 (1), 1–25. Available at: https://doi.org/10.1002/hbm.1058.

Norman-Haignere, S., Kanwisher, N.G., McDermott, J.H., 2015. Distinct cortical pathways for music and speech revealed by hypothesis-free voxel decomposition. Neuron 88 (6), 1281–1296. Available at: https://doi.org/10.1016/j.neuron.2015.11.035.

Nourski, K.V., et al., 2014. Spectral organization of the human lateral superior temporal gyrus revealed by intracranial recordings. Cereb. Cortex 24 (2), 340–352.

Pantev, C., et al., 1988. Tonotopic organization of the human auditory cortex revealed by transient auditory evoked magnetic fields. Electroencephalogr. Clin. Neurophysiology 69 (2), 160–170. Available at: http://www.sciencedirect.com/science/article/pii/0013469488902118.

Pereira, C.S., et al., 2011. Music and emotions in the brain: familiarity matters. PLoS One 6 (11), e27241. Available at: https://doi.org/10.1371/journal.pone.0027241.

Picton, T.W., et al., 1974. Human auditory evoked potentials. I: evaluation of components. Electroencephalogr. Clin. Neurophysiol. 36, 179–190. Available at: http://www.sciencedirect.com/science/article/pii/0013469474901552.

Ponton, C., et al., 2002. Maturation of human central auditory system activity: separating auditory evoked potentials by dipole source modeling. Clin. Neurophysiol. 113 (3), 407–420. Available at: http://www.sciencedirect.com/science/article/pii/S1388245701007337.

Puschmann, S., Huster, R.J., Thiel, C.M., 2016. Mapping the spatiotemporal dynamics of processing task-relevant and task-irrelevant sound feature changes using concurrent EEG-fMRI. Hum. Brain Mapp. 37 (10), 3400–3416. Available at: https://doi.org/10.1002/hbm.23248.

Rauschecker, J.P., 2011. An expanded role for the dorsal auditory pathway in sensorimotor control and integration. Hear. Res. 271 (1–2), 16–25. Available at: http://www.sciencedirect.com/science/article/pii/S0378595510003813.

Rauschecker, J.P., Scott, S.K., 2009. Maps and streams in the auditory cortex: nonhuman primates illuminate human speech processing. Nat. Neurosci. 12 (6), 718–724. Available at: https://doi.org/10.1038/nn.2331.

Rauschecker, J.P., Tian, B., 2000. Mechanisms and streams for processing of “what” and “where” in auditory cortex. Proc. Natl. Acad. Sci. 97 (22), 11800–11806. Available at: http://www.pnas.org/content/97/22/11800.abstract.

Rees, A., Palmer, A., 2010. The Oxford Handbook of Auditory Science: the Auditory Brain. Oxford university press.

Reznik, D., Ossmy, O., Mukamel, R., 2015. Enhanced auditory evoked activity to self-generated sounds is mediated by primary and supplementary motor cortices. J. Neurosci. 35 (5), 2173 LP–2180. Available at: http://www.jneurosci.org/content/35/5/2173.abstract.

Rose, J.E., et al., 1963. Some discharge characteristics of single neurons in the inferior colliculus of the cat. I. Tonotopical organization, relation of spike-counts to tone intensity, and firing patterns of single elements. J. Neurophysiol. 26 (2), 294 LP–320. Available at: http://jn.physiology.org/content/26/2/294.abstract.

Saenz, M., Langers, D.R.M., 2014. Tonotopic mapping of human auditory cortex. Hear. Res. 307, 42–52. Available at: https://doi.org/10.1016/j.heares.2013.07.016.

Scarff, C.J., et al., 2004. Simultaneous 3-T fMRI and high-density recording of human auditory evoked potentials. NeuroImage 23 (3), 1129–1142. Available at: http://www.sciencedirect.com/science/article/pii/S1053811904004082.

Schreiner, C.E., Langner, G., 1997. Laminar fine structure of frequency organization in auditory midbrain. Nature 388 (6640), 383–386.

Scott, S.K., Johnsrude, I.S., 2003. The neuroanatomical and functional organization of speech perception. Trends Neurosci. 26 (2), 100–107. Available at: http://www.sciencedirect.com/science/article/pii/S0166223602000371.

Shahin, A., et al., 2003. Enhancement of neuroplastic P2 and N1c auditory evoked potentials in musicians. J. Neurosci. 23 (13), 5545 LP–5552. Available at: http://www.jneurosci.org/content/23/13/5545.abstract.

Speckmann, E.J., Elger, C.E., 2004. Introduction to the neurophysiological basis of the EEG and DC potentials. In: Niedermeyer, E., Lopes da Silva, F. (Eds.), Electroencephalography: Basic Principles, Clinical Applications, and Related Fields. Lippincott and Williams.

Stockard, J.J., Rossiter, V.S., 1977. Clinical and pathologic correlates of brain stem auditory response abnormalities. Neurology 27 (4), 316. Available at: http://www.neurology.org/content/27/4/316.abstract.

Strainer, J.C., et al., 1997. Functional MR of the primary auditory cortex: an analysis of pure tone activation and tone discrimination. Am. J. Neuroradiol. 18 (4), 601 LP–610. Available at: http://www.ajnr.org/content/18/4/601.abstract.

Talavage, T.M., et al., 2004. Tonotopic organization in human auditory cortex revealed by progressions of frequency sensitivity. J. Neurophysiol. 91 (3), 1282 LP–1296. Available at: http://jn.physiology.org/content/91/3/1282.abstract.

Thomas, J.M., et al., 2015. Population receptive field estimates of human auditory cortex. NeuroImage 105, 428–439. Available at: https://doi.org/10.1016/j.neuroimage.2014.10.060.

Tzourio, N., et al., 1997. Functional anatomy of human auditory attention studied with PET. NeuroImage 5 (1), 63–77. Available at: http://www.sciencedirect.com/science/article/pii/S1053811996902529.

Vergani, F., et al., 2014. White matter connections of the supplementary motor area in humans. J. Neurol. Neurosurg. Psychiatr. 85 (12), 1377 LP–1385. Available at: http://jnnp.bmj.com/content/85/12/1377.abstract.

Walz, J.M., et al., 2015. Prestimulus EEG alpha oscillations modulate task-related fMRI BOLD responses to auditory stimuli. NeuroImage 113, 153–163. Available at: http://www.sciencedirect.com/science/article/pii/S1053811915002104.

Walz, J.M., et al., 2014. Simultaneous EEG-fMRI reveals a temporal cascade of task-related and default-mode activations during a simple target detection task. NeuroImage 102 (P1), 229–239. Available at: https://doi.org/10.1016/j.neuroimage.2013.08.014.

Walz, J.M., et al., 2013. Simultaneous EEG-fMRI reveals temporal evolution of coupling between supramodal cortical attention networks and the brainstem. J. Neurosci. official J. Soc. Neurosci. 33 (49), 19212–19222. Available at: http://www.ncbi.nlm.nih.gov/pubmed/24305817.

Wang, W., et al., 2016. Coupling between theta oscillations and cognitive control network during cross-modal visual and auditory attention: supramodal vs modality-specific mechanisms. PLoS One 11 (7), e0158465. Available at: https://doi.org/10.1371/journal.pone.0158465.

Warren, J.E., et al., 2006. Positive emotions preferentially engage an auditory–motor "mirror" system. J. Neurosci. 26 (50), 13067 LP–13075. Available at: http://www.jneurosci.org/content/26/50/13067.abstract.

Wessinger, C.M., et al., 1997. Tonotopy in human auditory cortex examined with functional magnetic resonance imaging. Hum. Brain Mapp. 5 (1), 18–25. Available at: http://dx.doi.org/10.1002/(SICI)1097-0193(1997)5:1<18::AID-HBM3>3.0.CO.

Wijers, B., 1995. Attention and brain function: R. Näätänen, erlbaum, Hillsdale, NJ, 1992. Acta Psychol. 89 (2), 189–192. Available at: http://www.sciencedirect.com/science/article/pii/0001691895900438.